npj | Quantum Materials

www.nature.com/npjquantmats

ARTICLE OPEN

Fulde–Ferrell–Larkin–Ovchinnikov and vortex phases in a layered organic superconductor

Shiori Sugiura[1], Takayuki Isono[1], Taichi Terashima[1], Syuma Yasuzuka[2], John A. Schlueter[3,4] and Shinya Uji[1,5]

Superconductivity is one of the most intriguing topics in solid state physics. Generally, the superconducting Cooper pairs are broken by the Zeeman effect, which gives the so-called Pauli paramagnetic limit H_{Pauli}. However, when the superconductivity is in the clean limit and the orbital effect is strongly quenched, the Cooper pairs can survive even above H_{Pauli}, which is the so-called Fulde and Ferrell, and Larkin and Ovchinnikov (FFLO) phase. Extensive efforts have been devoted to the discovery of the FFLO phase. However, vortex phase transitions have given rise to considerable ambiguity in the interpretation of the experimental data. Here, we report comprehensive magnetocaloric and torque studies of the FFLO phase transition in a highly two-dimensional organic superconductor. We observe the FFLO phase transition clearly distinct from vortex melting transitions. The phase diagram provides crucial information on the stability of the FFLO phase in magnetic fields.

npj Quantum Materials (2019)4:7 ; https://doi.org/10.1038/s41535-019-0147-2

INTRODUCTION

In layered organic superconductors, the perpendicular coherence length is comparable to the interlayer spacing. Therefore, the layered structures can be modeled as stacks of Josephson junctions. When the field is applied parallel to the layers, the orbital effect against superconductivity is strongly quenched, which is the main reason of the anisotropic upper critical field (H_{c2}). In addition, the superconductivity is in a clean limit for most of organic superconductors. The above two conditions, the quenched orbital effect and clean-limit superconductivity, are particularly favorable for the emergence of a novel superconducting (SC) phase, the so-called FFLO phase.[1,2] For conventional superconductors, the Zeeman effect breaks the superconductivity, giving the Pauli paramagnetic limit H_{Pauli}.[3] However, the FFLO superconductivity can survive even above H_{Pauli} sufficiently below T_c in parallel fields.

The FFLO transition from the homogeneous (conventional) SC phase is expected to occur at ~H_{Pauli}. In the FFLO phase, the Cooper pairs are formed between the up and down spins on the polarized Fermi surfaces and, consequently, have a non-zero center-of-mass momentum $\boldsymbol{q}$, which leads to an order parameter oscillation (periodic nodal lines) in the real space, $\Delta = \Delta_0 \cos(\boldsymbol{qr})$.[1,2]

In the last decade, extensive efforts have been devoted to the discovery of the FFLO phase in various layered superconductors,[4–21] which are the best candidates for FFLO phase studies. At the FFLO phase transition, the formation of the nodal lines in the SC layers inevitably leads to a vortex reconfiguration. On the other hand, in highly two-dimensional (2D) superconductors, each flux line can be decomposed into two parts, pancake vortex (PV) in the SC layer and Josephson vortex (JV) penetrating in the insulating layers between the SC layers. Depending on the field strength and direction, these vortex states are expected to show melting and layer decoupling, which make difficult to identify the FFLO transition unambiguously. Especially, no direct observation of the JV melting has led to controversial interpretation of the phase diagram.[7,11,13,17] Among various thermodynamic quantities, it is known that magnetocaloric effect (MCE) is quite sensitive to field-induced phase transitions. Therefore, the MCE is a powerful tool to investigate the FFLO transition as well as the vortex phase transitions.

The organic superconductor β″-(BEDT-TTF)$_2$SF$_5$CH$_2$CF$_2$SO$_3$ with the critical temperature $T_c \approx 5$ K, where BEDT-TTF stands for bis(ethylenedithio)tetrathiafulvalene, has a layered structure composed of the BEDT-TTF conducting and SF$_5$CH$_2$CF$_2$SO$_3$ insulating layers (Fig. 1).[22] Because of the large SF$_5$CH$_2$CF$_2$SO$_3$ anion, the energy band formed by the BEDT-TTF molecular orbitals is highly 2D. In this study, we performed systematic magnetic torque and MCE measurements. Especially from the MCE measurement, we successfully determine the FFLO phase and the vortex melting transitions separately and make the phase diagram as a function of field angle. The results provide an important step in the FFLO research.

RESULTS AND DISCUSSION

Figure 2a shows the field dependence of the magnetic torque at various temperatures for β″-(BEDT-TTF)$_2$SF$_5$CH$_2$CF$_2$SO$_3$ when the magnetic field is almost parallel to the layers ($\theta = -0.1°$). For highly 2D superconductors, the torque signal arises mainly from the perpendicular magnetization.[23] [See supplementary information (SI) A] Each torque curve exhibits a hysteresis between the up and down sweeps of the magnetic field, where the irreversibility fields (H_{irr}) can be defined (inset). The irreversible torque curve is caused by the strong pinning of the magnetic fluxes in the SC layers. The critical field H_{c2}, which should be slightly larger than H_{irr}, can not be determined without ambiguity because of the

[1]National Institute for Materials Science, Tsukuba, Ibaraki 305-0003, Japan; [2]Research Center for Condensed Matter Physics, Hiroshima Institute of Technology, Hiroshima, Hiroshima 731-5193, Japan; [3]Materials Science Division, Argonne National Laboratory, Argonne, IL 60439, USA; [4]Division of Materials Research, National Science Foundation, Alexandria, VA 22314, USA and [5]Graduate School of Pure and Applied Sciences, University of Tsukuba, Tsukuba, Ibaraki 305-8577, Japan
Correspondence: Shiori Sugiura (SUGIURA.Shiori@nims.go.jp) or Shinya Uji (UJI.Shinya@nims.go.jp)

Received: 22 June 2018 Accepted: 23 January 2019
Published online: 12 February 2019

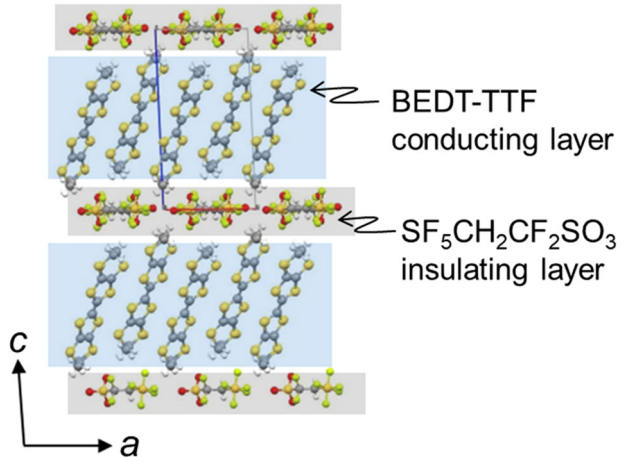

Fig. 1 Schematic of the crystal structure of β″-(BEDT-TTF)$_2SF_5CH_2CF_2SO_3$.[22] This salt is composed of the BEDT-TTF conducting and $SF_5CH_2CF_2SO_3$ insulating layers. Because of the large $SF_5CH_2CF_2SO_3$ anion, the energy band formed by the BEDT-TTF molecular orbitals is highly 2D

smooth variation above H_{irr}. The H_{irr} value decreases with increasing temperature. Figure 2b shows the torque curves at various field angles (θ) at 30 mK. The torque curve for $\theta = 1.8°$ has a flat part from ~1 T to ~11 T in Fig. 2b, which is qualitatively different from those at other angles. Similar torque behavior has been observed in other superconductors.[13,24] At such low angles, the cantilever bends so that the sample layer becomes almost parallel to the field, where most of the flux lines penetrate the insulating layers. This behavior, giving an almost constant torque in fields, is similar to a lock-in transition but the main origin is the tilting effect of the cantilever. As the field is tilted from the parallel direction, the hysteresis is reduced and H_{irr} decreases. In nearly perpendicular fields, we clearly see de Haas-van Alphen oscillations (inset). The result indicates clean-limit superconductivity, which is required for the FFLO phase. The frequency of the oscillation ($F \approx 200$ T) is consistent with previous results.[25]

Figure 2c presents the perpendicular diamagnetic susceptibility $-dM_z/dH_z$ as a function of field at various temperatures, obtained from the angular dependence of the torque (see SI A). The diamagnetic signals at all temperatures decrease with increasing field, which are associated with kinks indicated by arrows. The kink field H_{kink} is lower than H_{irr} for $T \leq 1.1$ K, which corresponds to the FFLO transition, as will be shown later.

Figure 3a shows the MCE in the down sweep at various magnetic field angles θ for the reference temperature $T_r = 80$ mK. The MCE ΔT is given by

$$\Delta T = -\tau \frac{d\Delta T}{dt} - \frac{T}{\kappa}\frac{dH}{dt}\left(\frac{\partial S}{\partial H}\right)_T + \delta T. \quad (1)$$

The first term shows thermal relaxation with a time constant $\tau = C/\kappa$, where C and κ are the heat capacity of the sample and addenda, and the thermal conductance between the sample and heat bath, respectively (see methods). In the second term, S is the magnetic entropy of the sample. The third term shows an additional heating arising from a latent heat and supercooling (or superheating) effect at a first-order phase transition or some other effects such as flux jumps. In the ΔT curves, we note three series of peaks. Only in a limited angle region ($|\theta| \lesssim 1.5°$), a broad peak (H_{peak1}) is observed at ~9.5 T, which is associated with a small hysteresis between the up and down sweeps (Fig. 3b). In general, ΔT changes the sign between the up and down sweeps due to the dH/dt term in Eq. (1). However, supercooling and superheating processes lead to positive ΔT for both sweeps (see SI B), which clearly shows that this is a first-order phase transition. As shown later, this peak is ascribed to the FFLO transition. Since the periodic nodal line structure is formed on the SC layers in the FFLO phase, the vortices will be reconfigured in the sample, which also causes heating for both sweeps.

When the field is tilted from the SC layers, we observe other two series of peaks associated with hysteresis, sharp and broad ones,

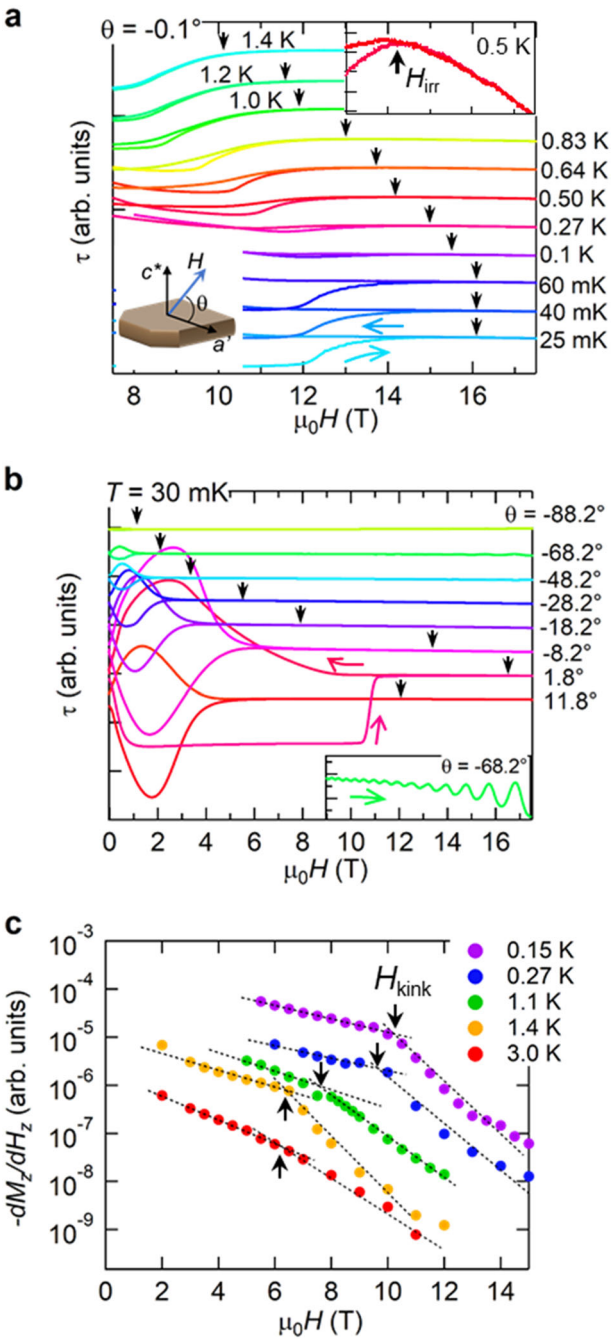

Fig. 2 Magnetic field dependence of the magnetic torque and diamagnetic susceptibility. **a** Torque curves at various temperatures. Each torque curve exhibits hysteresis between the up and down sweeps of the magnetic field, due to pinning of the flux lines. The irreversibility field (H_{irr}) is defined in the inset. **b** Torque curves at various field angles. The de Hass-van Alphen oscillations are observed at high fields (inset). **c** Magnetic field dependence of the diamagnetic susceptibility $-dM_z/dH_z$ at various temperatures. The $-dM_z/dH_z$ value is obtained from the angular dependence of the torque curve (see SI A). Arrows indicate the kink fields H_{kink}

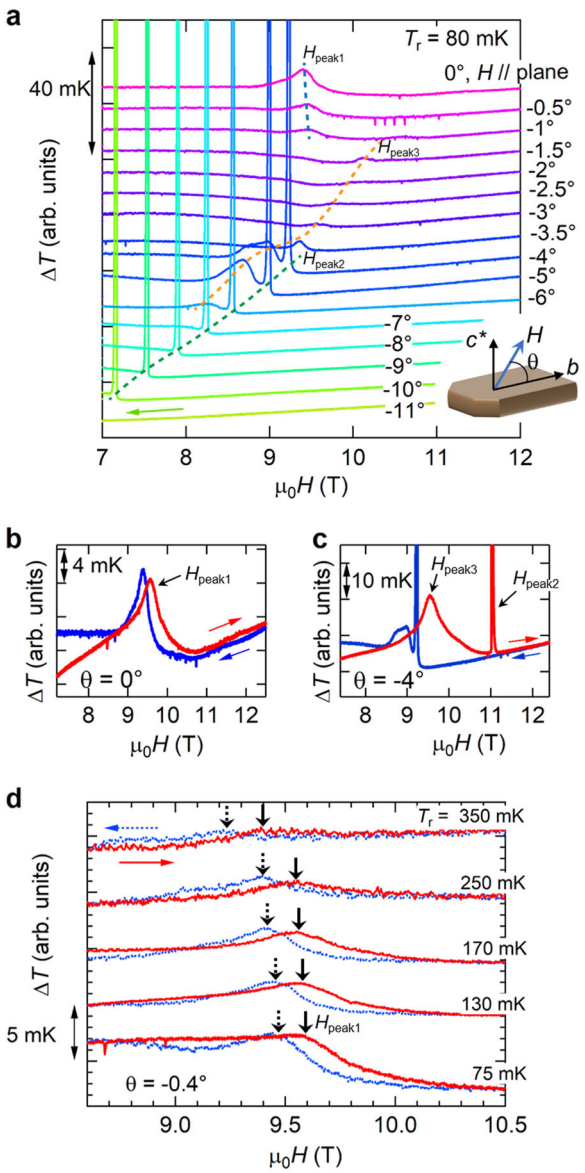

Fig. 3 MCE as a function of the magnetic field. **a** MCE as a function of the magnetic field at various field angles θ. Three series of peaks are observed. **b** A broad peak at H_{peak1} is observed only in a limited angle region. **c** Other two series of peaks, sharp and broad ones, which are denoted by H_{peak2} and H_{peak3}, respectively. All the peaks do not change the sign between the up and down sweeps, showing that supercooling and superheating effects are dominant at the transitions. **d** MCE as a function of the magnetic field at various temperatures. With increasing temperature, the peak field H_{peak1} indicated by arrows gradually decreases and the peak intensity is suppressed

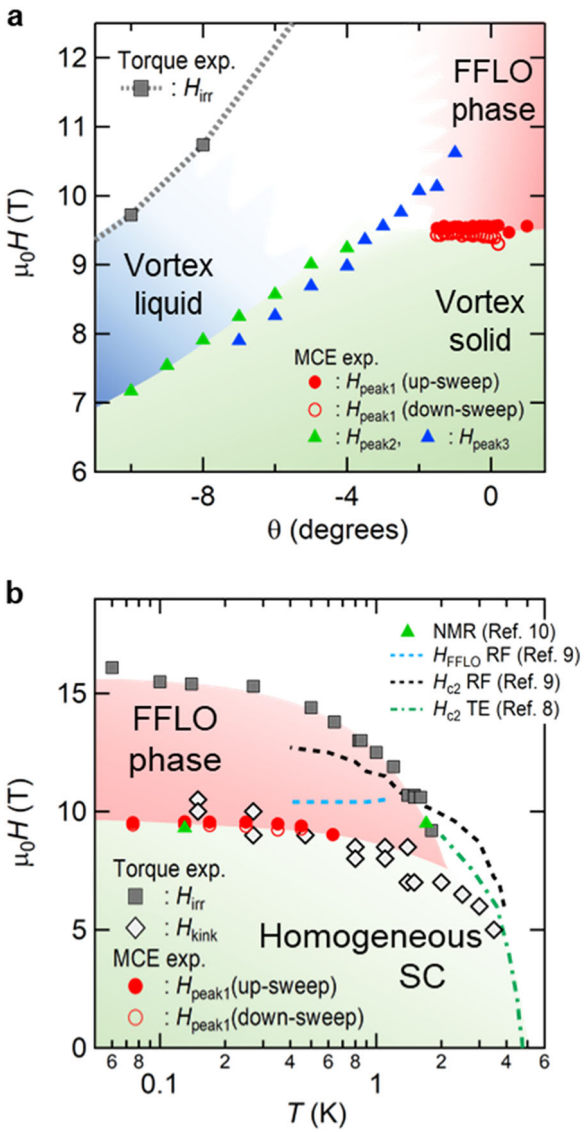

Fig. 4 Magnetic phase diagram. **a** H_{irr}, from the toque at 30 mK, and H_{peak1}, H_{peak2}, and H_{peak3} from the MCE at 80 mK are plotted as a function of the field angle. The irreversibility field H_{irr} rapidly increases as $\theta \to 0°$, showing cusp behavior of H_{c2}. Below H_{irr}, three MCE peaks at H_{peak1}, H_{peak2}, and H_{peak3} arise from the FFLO transition, melting transitions of the PVs and JVs, respectively. **b** H_{irr}, H_{kink}, and H_{peak1} are plotted as a function of temperature. Below 0.7 K, H_{peak1} agrees with H_{kink}, and both have a tendency to decrease with increasing temperature. The FFLO phase boundary decreases with increasing temperature down to ~8 T at ~2 K, where a tricritical point is present. For comparison, H_{FFLO} and H_{c2} determined by RF response[9] and thermal-expansion (TE) measurements[8] are also plotted

which are denoted by H_{peak2} and H_{peak3}, respectively (Fig. 3c). Similarly, both the peaks are ascribed to first-order phase transitions. We note that H_{peak2} and H_{peak3} show rapid increases as $\theta \to 0°$. The sharp peak at H_{peak2} suddenly vanishes at $\theta = 3.5°$. Similar angular dependence is observed at 1.7 K (see SI C). The dip/peak in the up/down sweep at 1.7 K clearly shows that the high field phase has a high magnetic entropy. The broad peak is observed at a lower field than the sharp peak. As $\theta \to 0°$, the intensity is suppressed but still visible at $\theta \approx 0°$.

Figure 3d shows the ΔT curves at various temperatures for $\theta = -0.4°$. With increasing temperature, the peak field H_{peak1} gradually decreases and the intensity is suppressed. When the field is perpendicular to the layer, we observe successive sharp spikes (rapid heating) due to flux jumps below H_{c2} (see SI D) and quantum oscillations (QOs) in the high field normal state (see SI E). The flux jumps are associated with precursor oscillations and overshoot cooling,[26] which are clearly distinct from the peaks at H_{peak1}, H_{peak2}, and H_{peak3}.

Figure 4a presents the field angle dependence of H_{irr}, H_{peak1}, H_{peak2}, and H_{peak3} obtained from the MCE measurements. The H_{irr} value rapidly increases as $\theta \to 0°$, corresponding to the cusp behavior of H_{c2}.[27] The magnetic field-temperature phase diagram is presented in Fig. 4b, where H_{irr}, H_{kink}, and H_{peak1} are plotted. Below ~0.7 K, H_{peak1} agrees with H_{kink}, and both have a tendency

to decrease with increasing temperature. H_{kink} rapidly decreases above ~2 K, and then approximately coincides with H_{c2} above ~2 K.[8] Since H_{irr} gives a lower limit of H_{c2}, we can conclude that there exists a phase boundary in the SC phase.

The observation of H_{peak1} in a very limited angle region (Fig. 4a) is consistent with the scenario of the FFLO transition; the FFLO phase is strongly destabilized by the orbital effect. The field dependence of the radio frequency (RF) response (resonance frequency change of a tunnel diode oscillator) shows an anomaly at ~10.5 T for $T = 0.45$ K.[9] The ^{13}C NMR measurement shows a kink at ~9.3 T in the relaxation rate for $T = 0.13$ K.[10] These features are interpreted as the FFLO phase transition, approximately consistent with the MCE peak at H_{peak1}. As the field increases, the perpendicular diamagnetism should be reduced at the FFLO phase because the flux lines can penetrate the sample along the nodes of the order parameter. Therefore, the kink in the $-dM_z/dH_z$ curve (Fig. 2c) also provide strong evidence of the FFLO transition.[16] The FFLO phase boundary is terminated at ~8 T and ~2 K, where a tricritical point exists.

The Clausius-Clapeyron relation at the FFLO phase transition is given by $\Delta S/\Delta M = -\partial H_{FFLO}/\partial T$, where ΔS and ΔM are the jumps of the entropy and magnetization at the FFLO transition field H_{FFLO}. The entropy jump at H_{FFLO} should be very small $\Delta S \approx 0$ since $\partial H_{FFLO}/\partial T \approx 0$ at low temperatures below ~0.4 K. Consequently, the latent heat $T\Delta S$ should also be small at H_{FFLO}. The MCE peak at H_{FFLO} arises predominantly from the δT term in Eq. (1). Since the heat capacity jump is given by $\Delta C = \partial \Delta S/\partial T$, it is very difficult to observe the FFLO transition in the heat capacity measurements. Above ~0.5 K, we see $\partial H_{FFLO}/\partial T < 0$ (Fig. 4b) and $\Delta M > 0$ (Fig. 2c) at H_{FFLO} as the field increases. Therefore, we conclude $\Delta S > 0$; the entropy in the FFLO phase is larger than that in the homogeneous SC phase. However, no sign reversal of the MCE signal at H_{FFLO} in the entire temperature range shows that ΔS is too small to detect.

In layered superconductors, the following two types of vortices are formed in tilted fields: PVs penetrating SC layers and JVs in insulating layers between the SC layers. We obtain $H_{c2}^{perp} = 1.3$ T[7] and $H_{c2}^{//} = 21.5$ T from the relation, $H_{c2}^{orb} = 0.7\partial H_{c2}(T)/\partial T|_{T=T_c}$.[28] These values give the coherence lengths, $\xi_{||} = 160$ Å and $\xi_{\perp} = 9.6$ Å. The $\xi_{\perp}$ value is shorter than the layer spacing $s = 17.5$ Å. Therefore, this salt is reasonably modeled as a Josephson coupled superconductor. The RF response measurements determine the anisotropy ratio $\gamma = 400$–800,[29] which gives the Josephson length $\lambda_J \approx 7000$–$14{,}000$ Å. The parallel penetration depth $\lambda_{||} \approx 10{,}000$ Å[29] is comparable to λ_J. Therefore, the PVs and JVs are expected to be well defined.[30] Actually, for a similar layered organic superconductor, κ-(BEDT-TTF)$_2$Cu(NCS)$_2$ with $\lambda_J \approx \lambda_{||}$, a lock-in transition is clearly observed, showing both JVs and PVs are well defined.[31] Therefore, the PV and JV picture will be reasonable for this salt.

At low temperatures and fields, where thermal fluctuation is suppressed, the PVs and JVs are likely in a solid phase. As field increases, the lattice constant $a_{PV} = \sqrt{\Phi_0/H}$ for the PV and $a_{JV} = \Phi_0/sH$ for the JV decreases, where Φ_0 and s are the flux quantum and layer spacing, respectively. When the mean-square amplitude of the vortex fluctuations in a solid phase becomes comparable to the lattice constant, the vortices melt.[32] This melting transition will take place even at zero temperature because of the quantum fluctuations. As field increases, the Josephson coupling between the layers is suppressed and the flux lines are highly entangled. Therefore, it is likely that the JVs melt first followed by the PVs; H_{peak2} and H_{peak3} are assigned to the melting transitions of the PVs and JVs, respectively. The JVs are confined in the insulating layers, showing a melting of the one-dimensional (1D) array, in contrast to the 2D melting for the PVs. In general, the fluctuation effect is more enhanced in a lower dimension system. It is probably the reason for the much broader melting transition of the JVs than that of the PVs. The sharp structure at H_{peak2} is similar to the previous specific heat measurement, which ascribes to the PVs melting transition.[13]

Recent resistance measurements on a highly layered organic superconductor, κ-(BEDT-TTF)$_2$Cu(NCS)$_2$ show that quantum and thermal fluctuations of the JVs cause peculiar energy dissipations at low temperatures. The results provide strong indications showing that the PVs and JVs melt separately; JVs first melt and then PVs melt with increasing field.[33] Since the order parameter is zero in the insulating layers, we expect that the JVs are highly fluctuating much more than the PVs. This is probably the main reason of the JVs melting at a lower field. Even when the PVs are pinning in the layers, the JVs can melt, which is described by a cutting and reconnecting process of the flux lines. For the decoupling between the PVs and JVs, highly 2D nature of the superconductivity is crucial.

Here, we briefly discuss the possibility of a lock-in transition at H_{peak3}. It is known that a lock-in transition takes place when the perpendicular field is comparable to the perpendicular lower critical field H_{c1} ($\cong 1$ mT).[34] The perpendicular component at H_{peak3} is an order of 0.1 T, which is two orders of magnitude higher than H_{c1}. In addition, the lock-in transition is theoretically of the second order,[30] which is consistent with torque measurements.[23] The hysteresis at H_{peak3} clearly demonstrates that the transition is of the first-order. A lock-in transition probably happens at a very low angle. However, we have not seen any sign of the lock-in transition in the magnetocaloric effect so far. The possible reason is that the entropy change of the lock-in transition is much smaller than those of the vortex melting transitions.

The H_{c2} value rapidly increases as $\theta \to 0°$, showing that both the Josephson coupling and order parameter are enhanced at a fixed field. Therefore, it will be reasonable that the melting transition fields of the PVs and JVs increase as $\theta \to 0°$. For $\theta \approx 0°$, we note that the H_{peak3} exceeds H_{peak1}; the JVs melt in the FFLO phase. The number of the PVs (n_{PV}) decreases as $\theta \to 0°$, proportional to $H \sin(\theta)$. The vanishing of H_{peak2} for $|\theta| < 4°$ in Fig. 3a and Fig. S3 (SI C) suggests that n_{PV} is lower than the dilution limit of the solidification.[35]

The temperature dependence of the heat capacity at high fields shows a peak below H_{c2} when the field is slightly tilted from the parallel direction.[11] As the field is tilted, the peak field decreases. From the comparison with our data, the heat capacity peak is the JV melting transition. In the NMR measurements, the ^{13}C relaxation rate in parallel fields has a small jump at 11 T above the FFLO transition for $T = 0.13$ K, whereas the Knight shift shows a smooth variation around 11 T.[10] The jump of the relaxation rate is also likely due to the JV melting.

METHODS

Single crystals of β″-(BEDT-TTF)$_2$SF$_5$CH$_2$CF$_2$SO$_3$ were synthesized by a standard electrochemical method.[22] The magnetic torque was measured by a piezoresistive micro-cantilever technique.[36] The MCE was measured by using a handmade semi-adiabatic cell as depicted in Fig. 5. Two thermometers (Lakeshore Cernox bare chips) are weakly thermally connected to the heat bath by thin Pt(W) wires of ϕ10 μm. A single crystalline sample of ~300 μg is attached to a thermometer (T_s) by an Apiezon N Grease. The other thermometer is used as a reference (T_r). The MCE ΔT is a thermal response of a sample to magnetic field change dH/dt, given by Eq. (1). When the magnetic entropy changes with field, the sample is heated or cooled due to the second and third terms. When the field sweep is stopped, the sample temperature is relaxed to the bath temperature ($\Delta T \to 0$) with the relaxation time τ. In this measurement, ΔT is defined as $\Delta T = T_s - T_r$. This technique enables us to cancel a drift of the bath temperature. The weak coupling between the thermometer and bath typically gives $\tau \approx 1$ s. All the MCE data shown here are taken at a sweep rate of 0.5 T/min. The cell is rotated in the field with a resolution of ~0.1°. All the measurements were made using a 20 T superconducting magnet with a dilution refrigerator at Tsukuba Magnet Laboratory, NIMS.

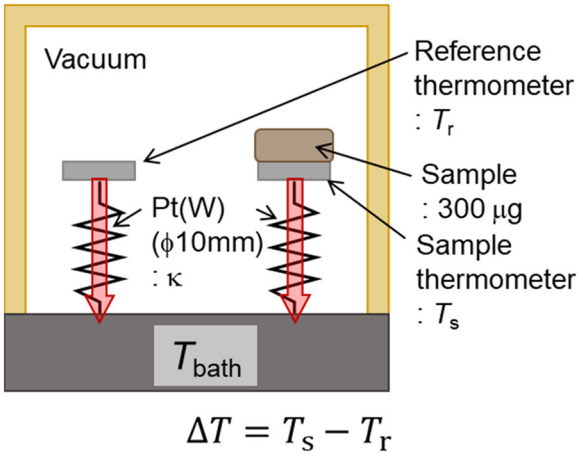

Fig. 5 Schematic picture of the vacuum cell for the MCE measurements

DATA AVAILABILITY

The data that support the findings of this study are available from the corresponding author on reasonable request.

ACKNOWLEDGEMENTS

S.U. acknowledges financial support from a Grant-in-Aid for Scientific Research from MEXT, Japan (No. 17H01144). Work at ANL was supported by UChicago Argonne, LLC, Operator of Argonne National Laboratory ("Argonne"). Argonne, a U.S. Department of Energy Office of Science laboratory, is operated under Contract No. DE-AC02-06CH11357. J.A.S. acknowledges support from the Independent Research/Development program while serving at the National Science Foundation.

AUTHOR CONTRIBUTIONS

S.S., T.T., and S.U. designed the experiments. S.S., T.I., and S.Y. mainly performed the measurements and analyzed the data. J.A.S. synthesized the single crystals. S.U. supervised the project.

ADDITIONAL INFORMATION

Supplementary information accompanies the paper on the *npj Quantum Materials* website (https://doi.org/10.1038/s41535-019-0147-2).

Competing interests: The authors declare no competing interests.

Publisher's note: Springer Nature remains neutral with regard to jurisdictional claims in published maps and institutional affiliations.

REFERENCES

1. Fulde, P. & Ferrell, R. A. Superconductivity in a strong-exchange field. *Phys. Rev.* **135**, A550–563 (1964).
2. Larkin, A. I. & Ovchinnikov, Y. N. Nonuniform state of superconductors. *Zh. Eksp. Teor. Fiz.* **47**, 1136–1146 (1964).[translation *Sov. Phys. JETP* **20**, 762 (1965).].
3. Clogston, A. M. Upper limit for the critical field in hard superconductors. *Phys. Rev. Lett.* **9**, 266–267 (1962).
4. Kamihara, Y., Watanabe, T., Hirano, M. & Hosono, H. Iron-based layered superconductor $La[O_{1-x}F_x]FeAs$ ($x = 0.05–0.12$) with $T_c = 26$ K. *J. Am. Chem. Soc.* **130**, 3296–6297 (2008).
5. Gurevich, A. Iron-based superconductors at high magnetic fields. *Rep. Prog. Phys.* **74**, 124501 (2011).
6. Terashima, T. et al. Hysteretic superconducting resistive transition in $Ba_{0.07}K_{0.93}Fe_2As_2$. *Phys. Rev. B* **87**, 184513 (2013).
7. Cho, C. et al. Thermodynamic evidence for the Fulde-Ferrell-Larkin-Ovchinnikov state in the KFe_2As_2 superconductor. *Phys. Rev. Lett.* **119**, 217002 (2017).
8. Müller, J. et al. Comparative thermal-expansion study of β″-$(ET)_2SF_5CH_2CF_2SO_3$ and κ-$(ET)_2Cu(NCS)_2$: Uniaxial pressure coefficients of T_c and upper critical fields. *Phys. Rev. B* **61**, 11739–11744 (2009).
9. Cho, K. et al. Upper critical field in the organic superconductor β″-$(ET)_2SF_5CH_2CF_2SO_3$: Possibility of Fulde-Ferrell-Larkin-Ovchinnikov state. *Phys. Rev. B* **79**, 220507(R) (2009).
10. Koutroulakis, G., Kühne, H., Schlueter, J. A., Wosniza, J. & Broun, S. E. Microscopic study of the Fulde-Ferrell-Larkin-Ovchinnikov state in an all-organic superconductor. *Phys. Rev. Lett.* **116**, 067003 (2016).
11. Beyer, R., Bergk, B., Yasin, S., Schlueter, J. A. & Wosnitza, J. Angle-dependent evolution of the Fulde-Ferrell-Larkin-Ovchinnikov state in an organic superconductor. *Phys. Rev. Lett.* **109**, 027003 (2012).
12. Singleton, J. et al. Observation of the Fulde-Ferrell-Larkin-Ovchinnikov state in the quasi-two-dimensional organic superconductor κ-$(BEDT\text{-}TTF)_2Cu(NCS)_2$ (BEDT-TTF ≡ bis(ethylene-dithio)tetrathiafulvalene). *J. Phys.: Condens. Matter* **12**, L641–L648 (2000).
13. Bergk, B. et al. Magnetic torque evidence for the Fulde-Ferrell-Larkin-Ovchinnikov state in the layered organic superconductor κ-$(BEDT\text{-}TTF)_2Cu(NCS)_2$. *Phys. Rev. B* **83**, 064506 (2011).
14. Agosta, C. C. et al. Experimental and semiempirical method to determine the Pauli-limiting field in quasi-two-dimensional superconductors as applied to κ-$(BEDT\text{-}TTF)_2Cu(NCS)_2$: Strong evidence of a FFLO state. *Phys. Rev. B* **85**, 214514 (2012).
15. Mayaffre, H. et al. Evidence of Andreev bound states as a hallmark of the FFLO phase in κ-$(BEDT\text{-}TTF)_2Cu(NCS)_2$. *Nat. Phys.* **10**, 928–932 (2014).
16. Tsuchiya, S. et al. Phase boundary in a superconducting state of κ-$(BEDT\text{-}TTF)_2Cu(NCS)_2$: Evidence of the Fulde–Ferrell–Larkin–Ovchinnikov phase. *J. Phys. Soc. Jpn.* **84**, 034703 (2015).
17. Agosta, C. C. et al. Calorimetric measurements of magnetic-field-induced inhomogeneous superconductivity above the paramagnetic limit. *Phys. Rev. Lett.* **118**, 267001 (2017).
18. Uji, S. et al. Magnetic torque studies on FFLO phase in magnetic-field-induced organic superconductor λ-$(BETS)_2FeCl_4$. *Phys. Rev. B* **85**, 174530 (2012).
19. Tanatar, M. A., Ishiguro, T., Tanaka, H. & Kobayashi, H. Magnetic field–temperature phase diagram of the quasi-two-dimensional organic superconductor λ-$(BETS)_2GaCl_4$ studied via thermal conductivity. *Phys. Rev. B* **66**, 134503 (2002).
20. Coniglio, W. A. et al. Superconducting phase diagram and FFLO signature in λ-$(BETS)_2GaCl_4$ from rf penetration depth measurements. *Phys. Rev. B* **83**, 224507 (2011).
21. Uji, S. et al. Vortex dynamics and diamagnetic torque signals in two dimensional organic superconductor λ-$(BETS)_2GaCl_4$. *J. Phys. Soc. Jpn.* **84**, 104709 (2015).
22. Geiser, U. et al. Superconductivity at 5.2 K in an electron donor radical salt of bis(ethylendithio)tetrathiafulvalene (BEDT-TTF) with the novel polyfluorinated organic anion $SF_5CH_2CF_2SO_3$. *J. Am. Chem. Soc.* **118**, 9996–9997 (1996).
23. Martinez, J. C. et al. Magnetic anisotropy of a $Bi_2Sr_2CaCu_2O_x$ single crystal. *Phys. Rev. Lett.* **69**, 2276–2279 (1992).
24. Kurita, N. et al. Determination of the upper critical field of a single crystal LiFeAs: The magnetic torque study up to 35 Tesla. *J. Phys. Soc. Jpn.* **80**, 013706 (2011).
25. Beckman, D. et al. Characterization of the Fermi surface of the organic superconductor β″-$(ET)_2SF_5CH_2CF_2SO_3$ by measurement of Shubnikov-de Haas and angle-dependent magnetoresistance oscillations and by electronic band-structure calculations. *Eur. Phys. J. B* **1**, 295–300 (1998).
26. Konoike, T. et al. Magnetothermal instability in the organic layered superconductor κ-$(BEDT\text{-}TTF)_2Cu(NCS)_2$. *Phys. Rev. B* **79**, 054509 (2009).
27. Zuo, F. et al. Low temperature upper critical field studies in organic superconductor β″-$(BEDT\text{-}TTF)_2SF_5CH_2CF_2SO_3$. *J. Low Temp. Phys.* **117**, 516 (1999).
28. Werthamer, N. R., Helfand, E. & Hohenberg, P. C. Temperature and purity dependence of the superconducting critical field, H_{c2} III. Electron spin and spin-orbit effects. *Phys. Rev.* **147**, 295–302 (1966).
29. Prozorov, R. et al. Unusual temperature dependence of the London penetration depth in all-organic β″-$(ET)_2SF_5CH_2CF_2SO_3$ single crystals. *Phys. Rev. B* **63**, 052506 (2001).
30. Bulaevskii, L. N., Ledvij, M. & Kogan, V. G. Vortices in layered superconductors with Josephson coupling. *Phys. Rev. B* **46**, 366–379 (1992).
31. Mansky, P. A., Chaikin, P. M. & Haddon, R. C. Evidence for Josephson vortices in $(BEDT\text{-}TTF)_2Cu(NCS)_2$. *Phys. Rev. B* **50**, 15929–15944 (1994).
32. Ryu, S., Doniach, S., Deutscher, G. & Kapitulnik, A. Monte Carlo simulation of flux lattice melting in model high-T_c superconductor. *Phys. Rev. Lett.* **68**, 710–713 (1992).
33. Uji, S. et al. Quantum vortex melting and phase diagram in the layered organic superconductor κ-$(BEDT\text{-}TTF)_2Cu(NCS)_2$. *Phys. Rev. B* **97**, 024505 (2018).
34. Wanka, S. et al. Specific heat and critical fields of the organic superconductor β″-$(BEDT\text{-}TTF)_2SF_5CH_2CF_2SO_3$. *Phys. Rev. B* **57**, 3084–3088 (1998).
35. Blatter, G., Feigel'man, M. V., Geshkenbein, V. B., Larkin, A. I. & Vinokur, V. M. Vortices in high-temperature superconductors. *Rev. Mod. Phys.* **66**, 1125–1388 (1994).
36. Rossel, C. et al. Active microlevers as miniature torque magnetometers. *J. Appl. Phys.* **79**, 8166–8173 (1996).